Photorefractive properties of $KNbO_3$

Roger J. Reeves, Mahendra G. Jani, Bahaeddin Jassemnejad,* and Richard C. Powell
Center for Laser Research, Oklahoma State University, Stillwater, Oklahoma 74078-0004

Greg J. Mizell and William Fay
Virgo Optics, Inc., 6736 Commerce Avenue, Port Richey, Florida 34668
(Received 25 January 1990)

Several experimental techniques were used to characterize the photorefractive properties of $KNbO_3$. Continuous-wave excitation was used to study two-beam coupling and creation times of photorefractive gratings for both undoped and doped samples. The results show how different types of dopants affect the photorefractive sensitivity and material properties relevant to the photorefractive effect such as carrier mobility, trapping time, effective trap density, effective electro-optic coefficient, Debye length, and the sign of the dominant photocarrier. Picosecond pulse excitation was used to study fast nonlinear responses of undoped $KNbO_3$. Along with the trapped-charge photorefractive response observed at long times after the excitation pulses, it was also possible to observe nonlinear responses due to absorptive changes at intermediate times and an ultrafast response that may have contributions associated with bound-electron nonlinearities and with scattering from Nb^{5+}-ion hopping modes.

I. INTRODUCTION

Displacive ferroelectric crystals have the electro-optic properties necessary for producing photorefractive effects (PRE's). These light-induced changes in the refractive index of the material are the basis for many important devices in optical technology involving holographic storage, optical data processing, and phase conjugation.[1] $KNbO_3$ is predicted to have a high photorefractive sensitivity for materials of this class, but its properties have not been fully characterized.[2] The purpose of the research described here is to present new information about the photorefractive response of $KNbO_3$ crystals. The two most important aspects of this work are determining how the material properties change with different types of doping ions and showing how the nonlinear-optical response of the material evolves with time after picosecond pulse excitation.

The material properties associated with the PRE's are characterized using a spatial light intensity grating generated by the interference of two coherent laser beams. The photorefractive response is associated with mobile charge carriers which are produced by photoionization of trap levels in the bright regions and through drift and diffusion are subsequently retrapped at new regions in the crystal. This leads to the buildup of a space-charge field in the material which modulates the refractive index through the electro-optic effect. Since the magnitude of the index change is proportional to the absorbed energy, the PRE can be generated with weak light sources on long-time scales, but it requires very high fluences to produce the PRE's with fast laser pulses. Other mechanisms associated with free carriers, bound charges, absorption changes, and vibrational properties can produce competing nonlinear-optical responses. To understand the PRE response of a material, it is necessary to characterize the charge generation, relocation, and trapping processes as well as the effects of the competing nonlinear-optical processes. This can be accomplished by using a variety of experimental techniques which provide information over a wide range of response times and for samples with several different trap compositions. The results of this type of comprehensive investigation of $KNbO_3$ are described in the following sections.

Potassium niobate is a ferroelectric material with the perovskite type of crystal structure. At room temperature it has orthorhombic crystal symmetry of point group $mm2$, and the electro-optic coefficients of this material have been determined.[3] The various structural phases of $KNbO_3$ can be thought of as being derived from the cubic paraelectric phase by a series of distortions of the original cubic cell. For example, the orthorhombic distortion consists of a stretch of the original cube along one of the face diagonals (the cubic $\{110\}$ direction). The $\{110\}$ direction suffering a slight elongation is the direction of spontaneous polarization and is designated as the c axis of the principal cell. The remaining principal axes coincide with the other twofold rotation axes. Using the convention of previous work, we label the orthorhombic b axis as the direction parallel to the [010] axis of the original cubic cell. This is the only axis conserved through the phase transitions of the material.

Single crystals of high-optical-quality $KNbO_3$ were grown from high-temperature solutions using established techniques.[4] Both undoped crystals and crystals containing up to 1 mol% of Ta^{5+}, Na^+, Rb^+, or Fe^{3+} were grown and cut into samples of approximate dimensions $3\times3\times5$ mm^3. A discolorization was observed in all doped samples with the exception of Na:$KNbO_3$. Preliminary studies indicate that each dopant was uniformly incorporated in the crystal lattice at concentrations up to the 1 mol% level used in this study. The crystals were

x-ray oriented and poled.[4] Slight variations were observed in the x-ray Bragg angles and Curie temperature for the Ta:$KNbO_3$ sample. The most probable location of Ta^{5+} in the $KNbO_3$ lattice is the Nb^{5+} site while the Na^+ and Rb^+ ions are believed to occupy the K^+ site. Fe^{3+} has been previously studied and reported to occupy the Nb^{5+} site with the creation of free charge carriers.[5] Prior to poling, chemical polishing of doped and undoped samples revealed various domain-wall structures which could be readily observed on the surface with 8× magnification. In some cases, these observed surface pits and steps corresponded to visible domain imperfections within the bulk and in close proximity to the surface. After poling and repolishing, no evidence of domain structures at the surface could be observed.

II. RESULTS FOR CONTINUOUS WAVE EXCITATION

Laser-induced photorefractive gratings were written in undoped and doped $KNbO_3$ crystals using the 514.5-nm emission of a continuous-wave (cw) argon-ion laser. The photorefractive characteristics of the samples were studied using two types of experimental measurements: two-beam coupling and transient four-wave mixing (FWM).

A. Experimental

The experimental setup used for the beam coupling experiments is shown in Fig. 1(a). In these experiments one of the two beams used to write the grating is reduced in intensity and is designated as the probe beam. The pump- and probe-beam intensities were 820 mW/cm^2 and 5.3 mW/cm^2, respectively, and the pump beam was expanded to eliminate problems associated with nonuniformities of the light interference pattern. This experimental arrangement results in a grating thickness that is always equal to the crystal thickness independent of the crossing angle between the two beams. The intensity of the transmitted probe beam was measured with a photomultiplier tube and recorded on a strip chart recorder. The photorefractive gain was determined by recording the intensity change of the transmitted probe beam as the pump beam was cycled on and off.

In the four-wave mixing arrangement [Fig. 1(b)], the laser-induced grating was produced by two equal intensity pump beams with the same beam diameters. The grating properties were determined by using a weak (50 μW/cm^2) HeNe laser for the probe beam. The probe beam enters the sample in the opposite direction from the pump beams and is aligned for Bragg diffraction off the grating. A photomultiplier tube was used to detect the intensity of the diffracted probe beam and the signal was recorded on a digital oscilloscope. By chopping the pump beams on and off, the dynamics of grating formation were studied.

B. Results of two-beam coupling measurements

For some samples and experimental conditions, the charge relocation properties cause the refractive index grating to be out of phase with the incident light pattern.

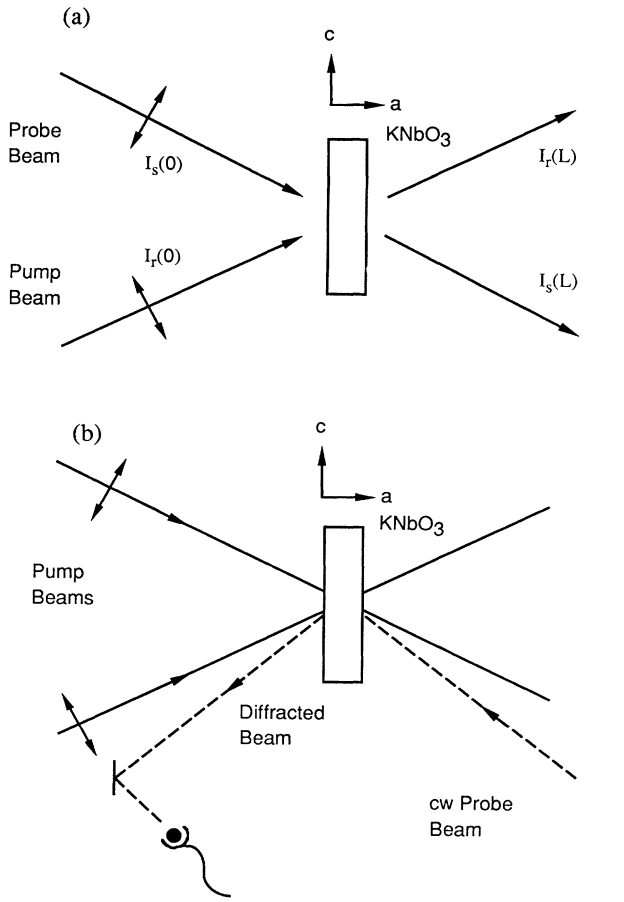

FIG. 1. Crystal and beam arrangements for (a) two-beam coupling experiments and (b) nondegenerate four-wave-mixing experiments.

Under these conditions energy can be transferred from one beam to the other. The direction of the energy transfer is determined by the crystal orientation and the sign of the dominant charge carrier. With the crystal oriented for maximum gain, the intensity of the signal beam can be written in terms of the gain coefficient Γ as[6]

$$\frac{I_s(L)}{I_s(0)}=\frac{[I_s(0)+I_r(0)]\exp[(\Gamma-\alpha)L]}{I_r(0)+I_s(0)\exp(\Gamma L)}, \tag{1}$$

where α is the absorption coefficient, L the interaction length, and I_r and I_s are the intensities of the pump and signal beams. Equation (1) reduces to

$$I_s(L)=I_s(0)\exp[(\Gamma-\alpha)L] \tag{2}$$

if $I_r(0)\gg I_s(0)$ and the pump beam is assumed to suffer negligible depletion traversing the length of the crystal. Experimentally we measure the effective gain[6] γ_0 given by

$$\gamma_0=I_s(L)_{\text{with pump}}/I_s(L)_{\text{without pump}}=\exp(\Gamma L) \tag{3}$$

if the depletion of the pump beam is neglected.

The beam coupling gain can be expressed in terms of

material parameters as

$$\Gamma = 2\pi n^3 r_{\text{eff}} E_{\text{SC}} / \lambda \ , \tag{4}$$

where n is the effective refractive index, r_{eff} is an effective electro-optic tensor component, and E_{SC} is the space-charge field. By including factors that account for the relative contributions of electrons and holes to the photorefractive effect, r_{eff} can be related to the electro-optic tensor component of a fully poled crystal as[7]

$$r_{\text{eff}} = F r_{\text{ang}} \sigma' \ . \tag{5}$$

F is a fractional poling factor, σ' is a normalized conductivity, and r_{ang} is the appropriate combination of electro-optic tensor components and angular and polarization factors for a fully poled crystal. For the two cases of only one type of charge carrier, $\sigma' = +1$ for holes and $\sigma' = -1$ for electrons. In the experiments performed here the two input beams were incident on the $\langle a \rangle$ surface of the crystal and were p-polarized so that r_{ang} can then be written as

$$r_{\text{ang}} = (n_3^4 r_{33} \cos^2\theta - n_1^4 r_{13} \sin^2\theta)/n^4 \ , \tag{6}$$

where

$$n = [(\cos^2\theta/n_3^2) + (\sin^2\theta/n_1^2)]^{-1/2} \ . \tag{7}$$

The space-charge field takes the form

$$E_{\text{SC}} = [2\pi k_B T/e][\Lambda_g/(\Lambda_g^2 + \Lambda_0^2)] \ , \tag{8}$$

where Λ_g is the grating spacing and

$$\Lambda_0 = [4\pi^2 \epsilon \epsilon_0 k_B T/(e^2 N_E)]^{1/2} \tag{9}$$

is the Debye screening length. Substituting for E_{SC} in Eq. (4) yields the expression for the photorefractive gain

$$\Gamma = [2\pi n^3 k_B T r_{\text{eff}}/(e\lambda)][K_g/(K_g^2 + K_s^2)] \ , \tag{10}$$

where $K_g = 2\pi/\Lambda_g$ and $K_s = 2\pi/\Lambda_0$. By measuring the beam gain Γ as a function of grating spacing Λ_g and applying Eq. (10), two material properties can be determined: r_{eff} and $N_E = NN^+/(N+N^+)$, the effective density of empty traps.

In all the beam coupling experiments on undoped and doped $KNbO_3$, the grating normal was aligned parallel to the c axis and the crystal and beam geometry were arranged to give gain to the signal beam. At each angle of the input beams, the effective gain γ_0 was measured and the photorefractive gain Γ determined using Eq. (3). The experimental values for Γ were fit to a straight line form[7] of Eq. (10),

$$K_g/\Gamma = [e\lambda/(2\pi n^3 k_B T r_{\text{eff}})][1 + (K_g^2/K_s^2)] \ , \tag{11}$$

with K_g/Γ plotted versus K_g^2. This presupposes that r_{eff} is independent of K_g. Examination of Eq. (5) shows that this assumption implies that σ' is independent of K_g, a situation that exists only if one type of photocarrier is dominant. When displayed in this manner, a value for r_{eff} can be obtained from the intercept and a value for K_s can be obtained from the slope and intercept of the straight-line plots. The experimental points are shown in Fig. 2(a) for the five crystals studied and the values of r_{eff} and N_E obtained from these results are summarized in Table I. Figure 2(b) shows theoretical curves of the photorefractive gain Γ as a function of grating spacing calculated using the values of r_{eff} and N_E in Table I. In calculating N_E from K_s and Eq. (9) a value of $\epsilon = 55$ was used.[8] Using a value[3] of $r_{\text{ang}} = r_{33} = 64$ pm/V, estimates of $F\sigma$ can be obtained giving some idea of the relative contributions of electrons and holes.

The direction of the photorefractive coupling is determined by the sign of the dominant photocarrier and the crystal and beam geometry. For each of the crystals studied the polarity of the c axis was determined in a pyroelectric cooling experiment[9] and the sign of the photocarrier determined from the results is listed in Table I.

C. Results of transient response measurements

Another important parameter of a photorefractive crystal is the time required to build up the refractive index grating. Reduced $KNbO_3$ has been shown to have a microsecond response time which greatly enhances its

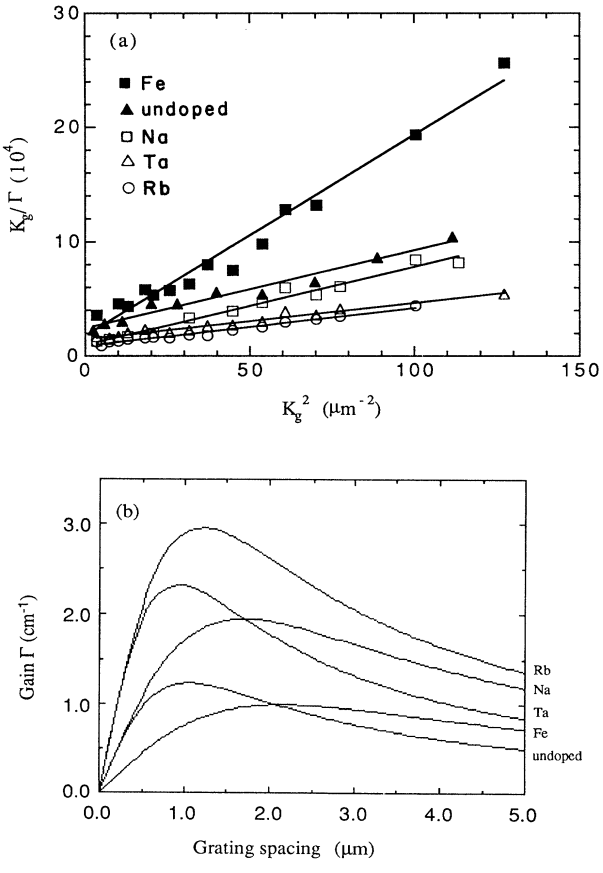

FIG. 2. (a) Grating wave vector K_g divided by beam coupling gain Γ as a function of K_g^2 for the five $KNbO_3$ crystals studied, and (b) theoretical curves of beam coupling gain Γ as a function of grating period using material parameters determined from least-squares fits to the data.

TABLE I. Material parameters obtained from two-beam coupling measurements on $KNbO_3$ crystals.

Crystal	Sign of dominant photo-carrier	Λ_0 (μm)	N_E (10^{16} cm^{-3})	r_{eff} (pm/V)	$F\sigma = r_{eff}/r_{33}$
$KNbO_3$ (undoped)	+	1.05	0.28	10.0	+0.20
$KNbO_3$:Ta	+	0.94	0.35	16.7	+0.33
$KNbO_3$:Rb	+	1.22	0.21	27.6	+0.55
$KNbO_3$:Fe	−	2.15	0.07	−16.4	−0.33
$KNbO_3$:Na	+	1.69	0.11	25.3	+0.15

potential for real time applications.[5]

Kukhtarev and co-workers[10,11] developed a mathematical analysis of the time evolution of the grating formation. This analysis has recently been extended for the case of dual charge carriers.[12,13] For fringe spacings large compared to both the charge diffusion length and the Debye screening length, the dielectric relaxation time

$$\tau_{di} = \epsilon\epsilon_0/(\sigma_d + \sigma_{ph}) \tag{12}$$

is a good approximation to the grating buildup time.[1] In Eq. (12) σ_d is the dark conductivity and σ_{ph} is the photoconductivity given by

$$\sigma_{ph} = e\alpha\Phi\mu\tau I/(h\nu) . \tag{13}$$

e is the electronic charge, α is the absorption coefficient, Φ is the quantum efficiency for exciting a charge carrier, μ is the mobility, I is the optical intensity, and $h\nu$ is the photon energy. Inverting Eq. (12) to give the grating buildup rate

$$\delta = (1/\tau_{di}) = (\sigma_d + \sigma_{ph})/(\epsilon\epsilon_0) \tag{14}$$

provides a linear relationship between I and δ. Using this approximation for the grating formation rate allows σ_{ph} to be determined from the slope of the fit of Eq. (14) to the data.

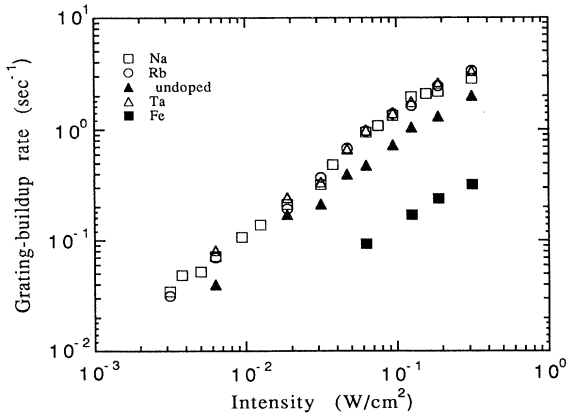

FIG. 3. Photorefractive grating buildup rate as a function of input light intensity for the five $KNbO_3$ crystals studied.

The grating buildup time was measured for all five crystals at one angle as a function of incident intensity. The buildup rate is plotted against light intensity in Fig. 3 for each crystal and the results are observed to qualitatively follow the straight-line model predicted by Eq. (14). The values of the product $\Phi\mu\tau$ obtained from the slopes are listed in Table II.

A useful figure of merit for characterizing the photorefractive sensitivity of a given material is how much optical energy is needed to produce a given refractive index change. Expressed in mathematical terms the sensitivity is[2]

$$S_n = \frac{dn}{d(\alpha W_0)} , \tag{15}$$

where n is the refractive index, α the absorption coefficient, and W_0 the incident optical energy. For a phase grating the diffraction efficiency is given by[14]

$$\eta = e^{(-\alpha d/\cos\theta)}\sin^2(d\pi\Delta n/\lambda\cos\theta) \tag{16}$$

and the induced refractive index change can be determined by measuring the absolute diffraction efficiency. The intensity of the scattered HeNe beam was calibrated to yield the absolute diffraction efficiency for all five crystals and combined with the grating buildup times to give the photorefractive sensitivity. The results obtained are given in Table II.

The results from the cw laser experiments show that doping $KNbO_3$ with Na^+, Rb^+, or Ta^{5+} at the 1 mol. % level enhances the photorefractive performances of the crystal. The maximum beam coupling gain and photorefractive sensitivity increases for these crystals over an

TABLE II. Material parameters obtained from FWM transient signal buildup rates measured on $KNbO_3$ crystals.

Crystal	S_n (10^{-5} cm^3/J)	$\Phi\mu\tau$ (10^{-10} cm^2/V)
$KNbO_3$ (undoped)	2.45	3.74
$KNbO_3$:Ta	3.79	6.46
$KNbO_3$:Rb	7.93	6.51
$KNbO_3$:Fe	0.41	0.53
$KNbO_3$:Na	3.22	6.07

undoped sample. The iron-doped crystal used in this study was observed to have an inferior photorefractive performance when compared to an undoped crystal. Also the predominant charge carrier was determined to be electrons in contrast to holes observed in the other crystals. Medrano *et al.*[15] found that the charge carriers in their iron-doped samples were holes and that there was an increase in photorefractive gain over a pure crystal that had been reduced and contained electrons as photocarriers. It is expected that it is the same Fe^{2+}-Fe^{3+} donor-trap system that produces the photorefractive effect in pure and iron-doped samples. Taken together, the results above suggest that it is the Fe^{2+}-Fe^{3+} ratio rather than absolute amounts that is important in predicting the photorefractive performance of a particular crystal.

III. RESULTS FOR PICOSECOND PULSE EXCITATION

The nonlinear optical response of $KNbO_3$ was investigated using picosecond pulses to establish laser-induced gratings. These gratings were probed using both picosecond and cw probe beams and the measurements obtained provide information on the time evolution of the gratings from a time scale of picoseconds out to many minutes.

A. Experimental

Single pulses with durations of 30 psec full width at half maximum (FWHM) at 532 nm were produced by a frequency-doubled, mode-locked Nd:YAG laser. After being split into two pump beams, the pulses were recombined in the crystal with an external crossing angle of 2θ. This angle could be varied from 16° to 44° corresponding to grating spacings varying from 1.91 to 0.71 μm. Typical incident energies of the two pump beams were 0.11 and 0.06 mJ giving an intensity modulation index of

$$m=2(E_1E_2)^{1/2}/(E_1+E_2)=0.95\ . \tag{17}$$

The diameter of each of the two pump beams was measured with a traveling knife edge and found to be 0.54 mm at the $1/e^2$ points of the on-axis peak intensity. The Gaussian radius of each beam is 0.27 mm and the incident fluences are 39 and 21 mJ/cm^2 for the two pulses. The temporal overlap of the two pump pulses was achieved with an optical delay line in one beam path.

A degenerate four-wave-mixing experiment was used to investigate the fast grating formation and decay. The experimental arrangement is shown in Fig. 4. A less intense, third picosecond pulse that was exactly counterpropagating to one of the pump beams acts as a probe beam. This probe pulse was *s*-polarized to be orthogonal to the pump-pulse polarization and was focused to the same diameter in the crystal. From phase matching considerations the diffracted signal is counterpropagating to the other pump beam and was extracted with a beam splitter. The arrival of the probe pulse in the crystal could be varied by an optical delay line. Delay times ranging from several hundred picoseconds before to several nanoseconds after the arrival of the pump pulses could be obtained. The diffracted signal was detected by the photodiode, recorded on a signal averager, and averaged over several thousand laser pulses.

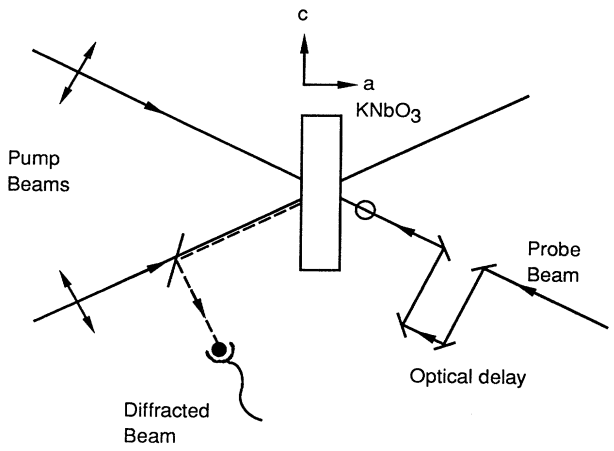

FIG. 4. Crystal and beam arrangements for the picosecond pulse-probe experiments on photorefractive gratings in $KNbO_3$.

In order to follow the signal to longer times, the probe pulse was replaced by a 1-mW cw He-Ne laser beam. The intensity of this laser was attenuated by three orders of magnitude to keep its influence below that required for grating erasure. The incident angle of the probe beam was adjusted to satisfy the Bragg scattering condition.

B. Results of pulse-probe measurements

The absolute diffraction efficiency was measured for gratings produced in $KNbO_3$ as a function of probe-pulse delay with the crystal in a photorefractive and in a nonphotorefractive geometry. The results are shown in Fig. 5 for a grating spacing that is 1.9 μm. In the pho-

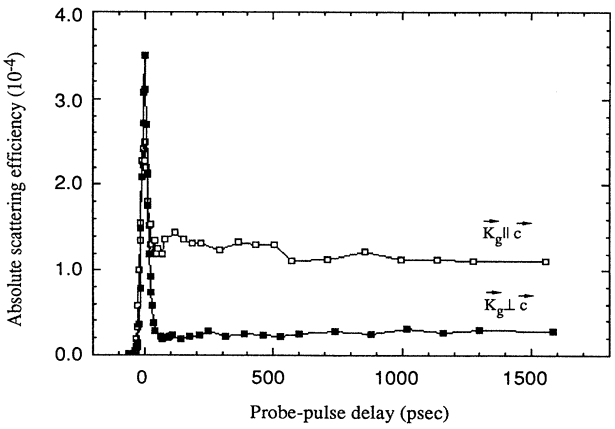

FIG. 5. Time evolution of the absolute scattering efficiency from a laser-induced grating written by two 30-psec pulses measured by an optically delayed weak probe pulse.

torefractive geometry the crystal is oriented with the grating wave vector $\mathbf{K}_g$ aligned parallel to the c axis of the crystal so the write beams produce an internal space-charge field that is also parallel to the c axis and the s polarized probe pulse senses the photorefractive effect through the r_{23} electro-optic tensor component. In the other geometry the crystal is rotated 90° ($\mathbf{K}_g \perp \mathbf{c}$) and any space-charge field produced will be in the direction of the crystallographic b axis. Due to the symmetry elements of the electro-optic tensor any index change produced will not be detected by an s-polarized probe pulse.

Two features are apparent in the data of Fig. 5 and they appear to be similar to results recently reported for $BaTiO_3$.[16,17] First a sharp peak is observed centered at a probe delay of $t=0$ psec. The real time width of this peak is close to the expected autocorrelation width of our three pulses. The origin of this signal is the fast physical processes contributing to the third-order susceptibility $\chi^{(3)}$ associated with the FWM of the two pump beams, probe beam, and signal beam. Possible contributions to the susceptibility include nonlinearities associated with bound electrons, free carriers, and any phonon or thermal effects with characteristic relaxation times comparable or less than the optical pulse width. In $BaTiO_3$, free carriers generated by single-photon absorption were thought to be the dominant contribution to the nonlinear susceptibility.[16,17]

The second feature apparent in Fig. 5 is a long-lived signal lasting for probe-pulse delays of several nanoseconds. It is more pronounced in the $\mathbf{K}_g \| \mathbf{c}$ orientation than in the $\mathbf{K}_g \perp \mathbf{c}$ orientation. This suggests that it may be photorefractive in origin. For this interpretation to be correct, impurity donor centers would have to be photoionized to produce free charge carriers that migrate far enough to establish a significant space-charge field during the time of the pump pulses. However, the small free carrier mobilities and fast trapping times that are typical of the ferroelectric oxides would allow the free carriers to diffuse only a small fraction of a grating spacing before being trapped. Thus there is some question about the origin of this component of the signal.

The intensity of the conjugate peak shows little change with grating spacing which is not the case for the signal at long probe-pulse delays. Figure 6 shows the intensity of the diffracted signal for four grating spacings. As the spacing decreases, the intensity of the nanosecond time component decreases. Such a decrease in a photorefractive grating is expected in high-mobility, long-trapping-time materials where the free carriers are able to destroy the grating by diffusing over a full grating period at small spacings before being trapped. However, in ferroelectric oxides the low mobilities coupled with the fast trapping times for charge carriers make this process unlikely. For the grating periods used in Fig. 6 the charge migration is expected to be diffusion dominated and the space-charge fields will be limited by the diffusion field

$$E_D = 2\pi k_B T/(e\Lambda_g) \ . \tag{18}$$

Thus the photorefractive effect will cause the intensity of the scattered signal to increase as the grating spacing decreases, which is exactly opposite to the results observed in Fig. 6. This casts further doubt on attributing this signal contribution to a photorefractive effect.

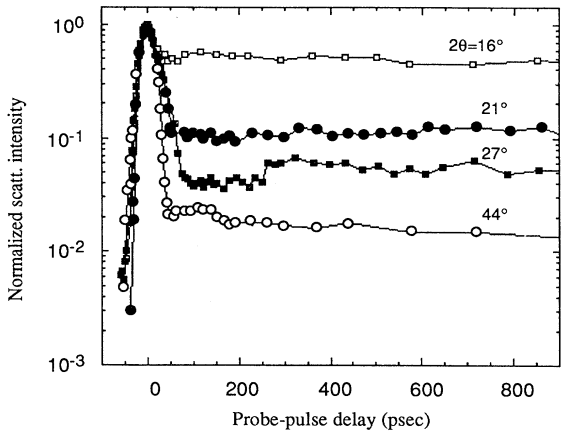

FIG. 6. Picosecond time evolution of the normalized scattering intensity for four grating spacings in $KNbO_3$.

In the results from the nonphotorefractive orientation shown in Fig. 5 there is a nonzero scattering background for long probe delays. This component may be associated with scattering from an absorption or photochromic grating generated by the photoexcitation and subsequent trapping of charge carriers. The diffraction efficiency for an absorption grating is given by[14]

$$\eta_a = (1-e^{-\alpha d})\sinh^2[\Delta\alpha d/(2\cos\theta)] \ . \tag{19}$$

The change in absorption coefficient $\Delta\alpha$ is just

$$\Delta\alpha = Ns \ , \tag{20}$$

where N is the density of displaced charges and s is the absorption cross section of the defect centers. The cw photorefractive beam coupling experiments showed that the concentration of donor centers in the crystal used here is $N_E = 3\times10^{15}$ cm^{-3}. Since the input photon rate is somewhat greater than this, we can approximate $N = N_E$. The absorption cross section of the donor levels is not known in $KNbO_3$, but some idea of its magnitude can be obtained from results in the literature. It is known that the most common defect center leading to photorefractive effects in as-grown ferroelectrics is the Fe^{2+}-Fe^{3+} system where the deep-level donor is Fe^{2+} and the acceptor is Fe^{3+}. The deep-level absorption cross section has been measured for this defect in InP:Fe and found to be[18] $s = 1\times10^{-17}$ cm^2. Using this value of s for $KNbO_3$ we obtain $\Delta\alpha = 0.03$ cm^{-1}. Substituting for $\Delta\alpha$ in Eq. (19) yields a diffraction efficiency of $\eta_a = 10^{-5}$ which is in good agreement with the observed scattering efficiency of about $\eta = 2\times10^{-5}$ for this signal component. The consistency of this interpretation of the $\mathbf{K}_g \perp \mathbf{c}$ results suggests that the $\mathbf{K}_g \| \mathbf{c}$ results might be associated with a directional-dependent change in the absorption coefficient.

Figure 7(a) shows the results of measuring the scatter-

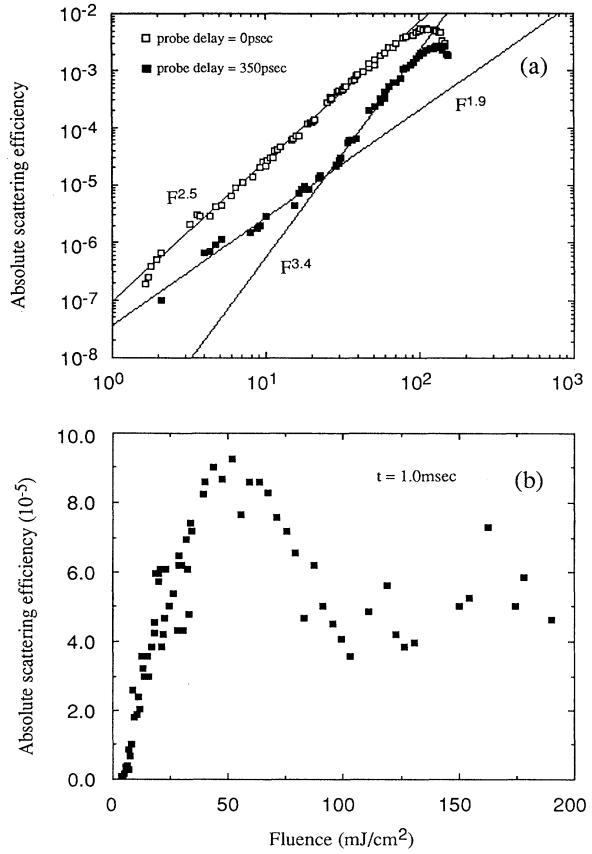

FIG. 7. Absolute scattering efficiency as a function of the fluence of two 30-psec writing pulses at (a) probe delays of 0 and 350 psec after the writing pulses and (b) at a time of 1.0 msec after the writing pulses as measured by a cw probe beam.

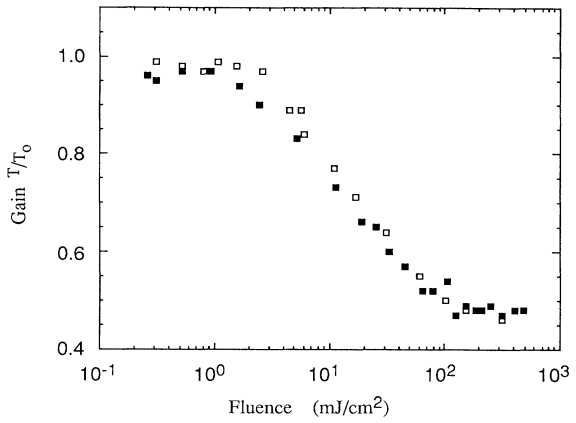

Fig. 8. Ratio of the probe-pulse intensity with the pump beam on T and the pump beam off T_0, as a function of incident fluence in a picosecond-pulse two-beam coupling experiment on $KNbO_3$. The closed and open squares represent the two photorefractive crystal orientations that are related by a 180° rotation about a line bisecting the two input beams.

ing efficiency as a function of incident fluence. At a probe-pulse delay of 0 psec, the diffraction efficiency follows a power-law dependence on the total fluence F of $F^{2.5}$, slightly greater than the quadratic dependence expected. At a delay time of 350 psec, a single power-law dependence is not observed. In the low-intensity region with fluences below 10 mJ/cm^2 a least-squares fit to the data yields a dependence of $F^{1.9}$. Above 10 mJ/cm^2 a power-law dependence of $F^{3.4}$ is observed. At both of these delays there is a saturation of the signal around an incident fluence of 100 mJ/cm^2.

A definite signature of the photorefractive effect is the observation of two-beam coupling. An experiment was performed to detect two-beam coupling in $KNbO_3$ using picosecond pulses and the results are shown in Fig. 8. The crystal was oriented in the photorefractive geometry with a grating spacing of 1.9 μm and a pump-beam--to-probe-beam intensity ratio of 9:1. The experimental quantity measured and plotted in Fig. 8 is the ratio T/T_0 as a function of the incident fluence, where T is the intensity of the transmitted probe beam with the pump beam on and T_0 is the intensity with the pump beam off. Energy transfer through photorefractive gain will increase the intensity of the probe beam in the presence of the pump beam. The points represented by closed and open squares correspond to the two photorefractive crystal orientations that are related by a 180° rotation about a line bisecting the two input beams. The photorefractive contribution to the signal will reverse direction when the crystal is rotated and be seen as a difference between the points for the two orientations in Fig. 8. Such a difference is not observed in these results suggesting that the free carriers do not diffuse the required half grating spacing on picosecond time scales. The decay in the ratio T/T_0 as a function of fluence is most probably associated with two-photon absorption.

In conjunction with these two-beam coupling measurements, the probe-pulse transmission was recorded as a function of the arrival time of the pump pulse. The results obtained are shown in Fig. 9 where the ratio T/T_0 is plotted against probe-pulse delay for the two crystal orientations $\mathbf{K}_g \| \mathbf{c}$ and $\mathbf{K}_g \perp \mathbf{c}$. This experiment was performed at the same crossing angle as the beam coupling results and the intensity of the pump beam was 80 mJ/cm^2. For negative probe-pulse delays, i.e., the probe pulse arrives before the pump pulse, the ratio T/T_0 is close to unity and there is no interaction between the beams. As the pulses start to overlap in time the probe is attenuated through two-photon absorption which peaks at zero delay. For both crystal orientations the probe pulse continues to be attenuated at long delay times after the pump pulse. The extend of the attenuation is significantly greater in the $\mathbf{K}_g \| \mathbf{c}$ orientation than in the perpendicular $\mathbf{K}_g \perp \mathbf{c}$ orientation. At these long-time scales there is no temporal overlap of the pulses and the effects are not grating or photorefractive in origin. A reasonable explanation of these results is the anisotropy of the absorption coefficient relative to the crystal c axis. Thus we conclude from these results that the contribu-

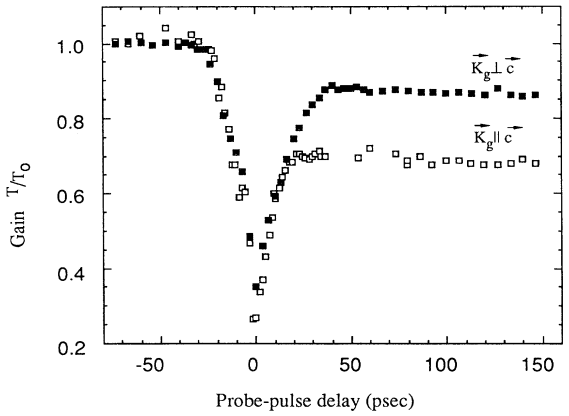

FIG. 9. The quantity T/T_0 as a function of the arrival time of the probe pulse for two orientations of a $KNbO_3$ crystal.

tion to the FWM signal on the time scale of several hundred picoseconds to nanoseconds after picosecond pulse excitation is due to a laser-induced absorption grating.

C. Results of cw probe measurements

The picosecond pulse experiments were repeated using a cw probe beam. In this case, the fast-time resolution of the pulse-probe experiments described in the previous section is lost, but the evolution of the signal can be followed to very long times. The transient signals obtained show the decay of the fast nonlinear responses and the buildup and dark decay of the photorefractive grating. The crystal *a* axis and the polarization of the probe beam were aligned in the plane of incidence (*p* polarization) so the effective electro-optic coefficient is given in Eq. (6). The signal was followed in time after a single 30-psec pulse of excitation from the crossed write beams.

Figure 10 shows the time evolution of the scattering efficiency for different excitation fluences. The intensities of the fast- and long-time components of the signal change differently with fluence and the buildup time of the long-time signal decreases as fluence is increased. Figure 7(b) shows the results of measuring the signal strength at 1 msec after the write pulses as a function of write-beam fluence. The data show a very different behavior than the signals measured at faster times shown in Fig. 7(a). The observed behavior does not fit a single power-law dependence but is close to linear below 50 mJ/cm^2 at which point the scattering efficiency is observed to saturate.

Figure 11 shows the dark decay of photorefractive

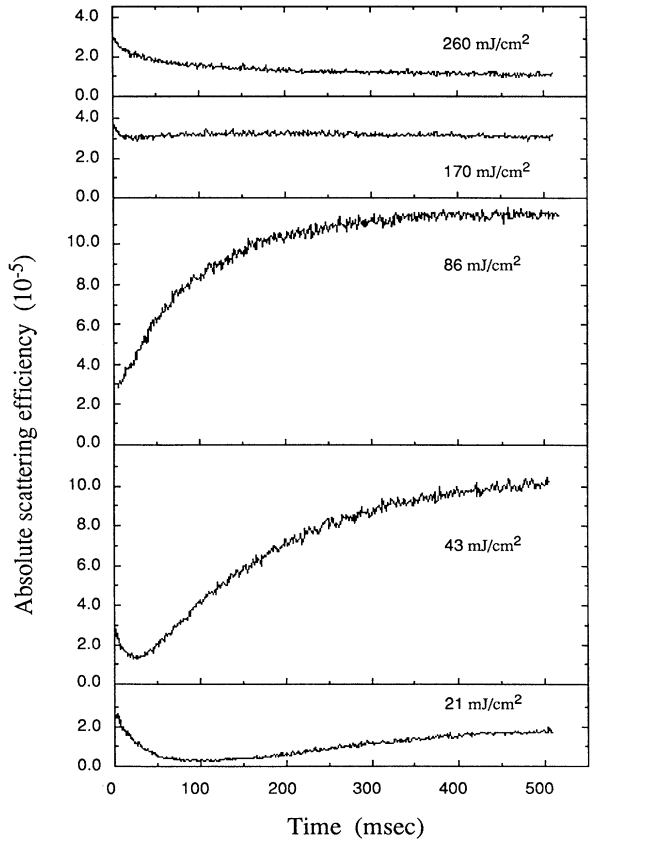

FIG. 10. Time evolution of the absolute scattering efficiency of laser-induced gratings in $KNbO_3$ as a function of time after the arrival of the two 30-psec writing pulses measured by a cw probe beam.

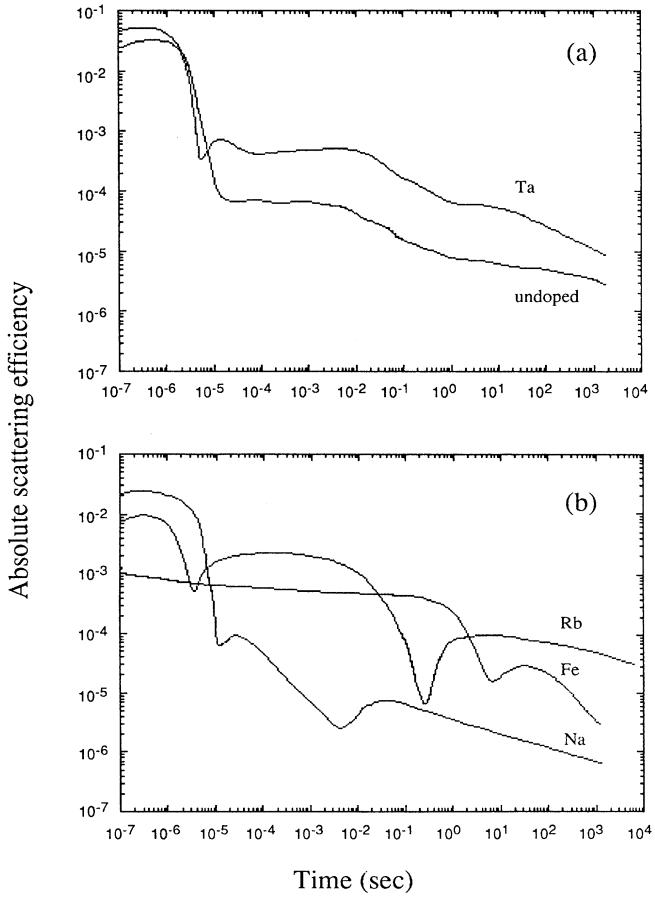

FIG. 11. Dark decay of photorefractive gratings in doped $KNbO_3$ crystals induced by two single 30-psec writing pulses.

gratings written by single laser pulses in the doped and undoped $KNbO_3$ crystals. The signal for the undoped crystal has at least two decay components with very different relaxation times. Nonexponential erasure decays have been observed in $Bi_{12}SiO_{20}$ (Ref. 19) and $LiNbO_3$ (Ref. 20) and were explained by the participation of several trapping centers in the photorefractive charge migration. Steady-state beam coupling results presented earlier show that both electrons and holes are involved in the photorefractive processes in the crystals used here. The decay results observed demonstrate that the trapping mechanism involves two types of acceptors that have two distinct relaxation times. One trap may be associated with the creation of holes in the valence band by photoexcitation of electrons to midgap impurity levels, while the other may be associated with photoexcitation of electrons to the conduction band. It is well known that mobilities of electrons and holes are different in these types of materials and multiple components to the decay of a grating involving both electrons and holes should be expected.

The doped $KNbO_3$ crystals show more complicated dark decays. In some cases the intensity of the scattered beam is observed to undergo several dips where one component of the grating decays while another component with a longer relaxation time still contributes to the intensity. Theoretical modeling of these features will require incorporation of multiple trapping levels in describing the dynamics of charge relocation.

Figure 12 shows the dark decay of the photorefractive grating in undoped $KNbO_3$ for five different grating spacings. The decay time decreases with grating spacing reflecting the shorter time charge carries require to diffuse a half grating period. The nonexponential nature of the decay is more pronounced for the smaller grating spacings. For the larger spacings the decay is expected to be dominated by the carrier with the highest mobility and a single exponential decay would result. As the spacing decreases both carriers and their respective trapping centers are able to contribute to the decay and nonexponential transients appear.

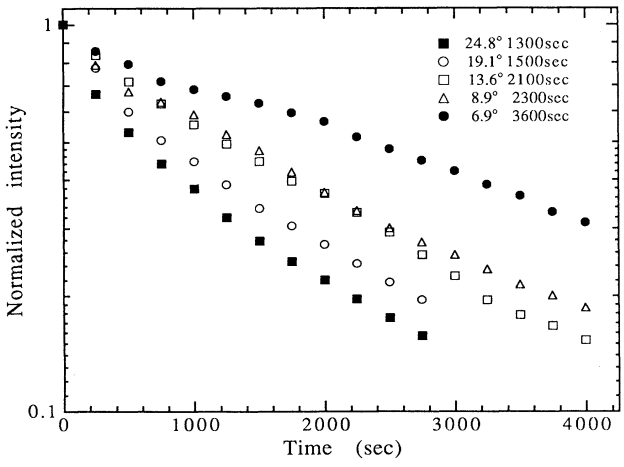

FIG. 12. Dark decay of photorefractive gratings in $KNbO_3$ for five different grating periods.

IV. DISCUSSION AND CONCLUSIONS

Characterization of the photorefractive effect using cw excitation has been reported previously for $KNbO_3$ crystals where the response time for reduced $KNbO_3$ was measured to be 100 μsec.[5] Also, doping with iron has been shown[15] to result in a substantial increase in the photorefractive efficiency over that of undoped samples. The results described here using cw excitation give a further understanding of the photorefractive effect in doped and undoped $KNbO_3$ by determining various material parameters associated with laser-induced charge relocation. The mobility-lifetime products given in Table II show that doping $KNbO_3$ with either Ta, Rb, or Na decreases the time required to form a photorefractive grating by a factor of 2 over an undoped crystal. This increase in the buildup rates carries over to an enhancement in the photorefractive sensitivity for these crystals with the Rb dopant producing the highest. In the Fe-doped sample electrons were found to be the dominant charge carrier while holes were the dominant carriers in all other samples.

It is only recently that picosecond pulses have been used to study nonlinear responses of materials such as $Bi_{12}SiO_{20}$,[21] $BaTiO_3$,[16,17] GaAs,[22] and CdTe.[23] In the picosecond work reported here on $KNbO_3$, three different types of nonlinear effects were identified due to their different time responses. Utilizing both pulsed and cw probe beams, picosecond laser-induced grating techniques were used to follow the evolution of the nonlinear response from the picosecond time scale out to times of many minutes. On the time scale of milliseconds and longer, the photorefractive response which was observed with cw excitation is seen. This is associated with the space-charge field built up by photoinduced charge relocation and the interaction of this field with the electro-optic tensor components of the material. The dark decay of the signal is highly nonuniform indicating that different types of traps are taking part in the charge relaxation back to an equilibrium configuration.

On the time scale of 100 psec out to nanoseconds, the nonlinear response has properties that are better described by a laser-induced change in the absorption coefficient associated with two-photon absorption. The time scale and magnitude of this signal are consistent with a relocation of charge carriers. For example, since the dominant photoinduced charge carriers are holes, the first photon might create a hole by promoting an electron in the valence band into a midgap acceptor. The second photon might promote this electron into the conduction band. The electrons and holes created in this way will migrate to different types of traps before finally recombining.

The variation of the signal in this time regime for different crystal orientations is associated with the anisotropy of the absorption coefficient. The absorption coefficient for $KNbO_3$ is a tensor quantity with different values for different propagation and polarization direc-

tions. If a, b, and c are the crystallographic axes, then the absorption coefficient can be represented by the tensor

$$\alpha=\begin{bmatrix} 0 & \alpha_{ab} & \alpha_{ac} \\ \alpha_{ab} & 0 & \alpha_{ac} \\ \alpha_{ca} & \alpha_{ca} & 0 \end{bmatrix} , \tag{21}$$

where α_{ij} is the absorption coefficient for a beam propagating in the ith direction with polarization along the j axis. If the crystal is oriented with $\mathbf{K}_g \| \mathbf{c}$, the probe-pulse polarization is always perpendicular to the c axis and the apparent absorption coefficient is given by the linear combination

$$\alpha=\alpha_{ab}\cos\theta+\alpha_{ca}\sin\theta , \tag{22}$$

where θ is the half-angle between the intersecting pump and probe beams. In the orthogonal orientation $\mathbf{K}_g \perp \mathbf{c}$, the appropriate combination for the absorption coefficient is

$$\alpha=\alpha_{ac}\cos\theta+\alpha_{ac}\sin\theta . \tag{23}$$

For the data in Fig. 9, $\theta=8°$ and the attenuation of the probe in the $\mathbf{K}_g \perp \mathbf{c}$ orientation is due mainly to the first term in Eq. (23). The first term in Eq. (22) is expected to be of this same magnitude and the extra attenuation of the probe in the $\mathbf{K}_g \| \mathbf{c}$ orientation is due to the component $\alpha_{ca}\sin\theta$. As the angle θ increases the probe beam in both the two-beam coupling experiment and in the FWM experiment will undergo an increasing absorption as it propagates more along the c axis. This is consistent with the results shown in Fig. 5. Based on this analysis, the longer-lived signal in the picosecond pulse-probe FWM experiments is the scattered beam from an absorption grating. The photoexcited charge carriers are trapped on a time scale comparable with the optical pulse width but their redistribution among different trapping levels sets up an absorption grating that is anisotropic with crystallographic directions.

The physical origin of the fast conjugate peak observed in the picosecond FWM experiments is difficult to determine unambiguously because its time response cannot be resolved with 30-psec pulses used here. This signal is associated with the third-order susceptibility of the material and can have contributions from electronic and vibrational mechanisms that respond on a picosecond time scale. The extend of each contribution can be estimated from the nonlinear refractive index for the effect. If the induced change in the refractive index is Δn, the nonlinear refractive index n_2 is defined as[24]

$$\Delta n=n_2\langle E^2\rangle , \tag{24}$$

where E is the electric field of the optical wave. n_2 is related to the third-order susceptibility by[24]

$$n_2=(12\pi/n_0)\chi^{(3)} , \tag{25}$$

where n_0 is the background refractive index which equals 2.35 for $KNbO_3$. For a refractive index grating, the theory of Kogelnik[14] can be used to obtain the refractive index change induced from the absolute scattering intensity by

$$\Delta n=(\lambda\cos\theta/\pi d)\sqrt{\eta} . \tag{26}$$

The maximum diffraction efficiency recorded in these experiments at $\Delta t=0$ was $\eta=5.5\times10^{-3}$ obtained at an intensity of 100 mJ/cm^2. The electric-field intensity of the incident wave is related to the fluence F by[25]

$$\langle E^2\rangle=(8\pi/cn_0)F=1.19\times10^7 \tag{27}$$

for the above fluence, in cgs units. The value of $\chi^{(3)}$ measured in this case is calculated to be 2.3×10^{-13} esu.

Two of the electronic contributions to the conjugate peak will be scattering from a free-carrier index grating that is generated by single-photon absorption and scattering from the induced polarization of bound charges in the material. The change in the refractive index associated with scattering from a free-carrier grating is given in the Drude model by[26]

$$\Delta n=2\pi N_c e^2/(n_0\nu^2 m_c) , \tag{28}$$

where N_c is the density of free carriers of effective mass m_c. N_c (in cm^{-3}) can be approximated by the absorbed photon flux

$$N_c=(\lambda\alpha/hc)I=5.4\times10^{16} . \tag{29}$$

Using this value in Eq. (28) predicts the free-carrier grating index change and third-order susceptibility contribution to be $\Delta n=3.0\times10^{-6}$ and $\chi^{(3)}=1.5\times10^{-14}$ esu. These are an order of magnitude smaller than the measured values.

The value of $n_2=29\times10^{-13}$ esu measured[27] for $KTaO_3$ can be used as an approximation for the bound-charge contribution to $\chi^{(3)}$ for $KNbO_3$. Using Eq. (25) the third-order nonlinear susceptibility from this effect is calculated to be 1.8×10^{-13} esu, which is the same order of magnitude as the measured value.

Recent Raman-scattering experiments on $KNbO_3$ have shown central peaks in the scattering spectrum that are associated with relaxation modes involved in the successive cubic-tetragonal-orthorhombic-rhombohedral phase transitions.[28,29] While there is some question about an additional contribution to the signal from a soft phonon mode, this is not relevant to the results described here.[30,31] It is beyond the scope of our experiments to resolve the specific contributions due to the relaxation modes and soft modes. However, it is clear that the Nb^{5+} relaxation modes are responsible for a contribution to the dielectric constant of the material and thus will contribute to the nonlinear refractive index measured as a conjugate signal peak in our FWM experiments.

The multiwell potential surface involved with the hopping modes is the eight-site order-disorder model used to describe the successive phase transitions in displacive ferroelectric crystals.[28] This model has the Nb^{5+} ions located in one of eight potential wells which have potential minima displaced from the cubic unit cell center along the $\langle 111\rangle$ directions. The different structural phases of the crystal are a consequence of the preferential occupation by the Nb^{5+} ion of a certain set of potential wells.

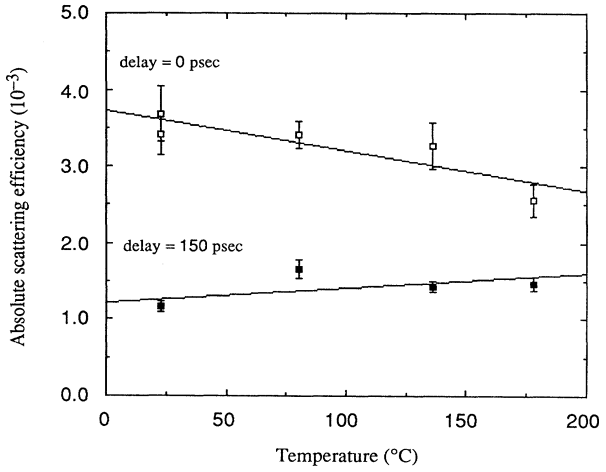

FIG. 13. Absolute scattering efficiency of a laser-induced grating in $KNbO_3$ as a function of temperature for probe-pulse delays of 0 and 150 psec after the 30-psec writing pulses.

For example, in the cubic phase each of the eight sites is equally occupied, while tetragonal ordering arises below the first phase transition temperature due to a set of four wells perpendicular to a particular axis becoming preferentially occupied.

The influence of this polar hopping mode on the laser-induced gratings is very similar to the analysis of stimulated Raman scattering. However in this case the low frequency of the mode means the effect is seen in a degenerate mixing configuration. The contribution to $\chi^{(3)}$ can be calculated using fluctuation-dissipation theory arriving at the result[32]

$$\chi^{(3)}=-(N/8h)[(v\alpha_k^2)/(v^2+\omega^2)] . \quad (30)$$

The polarizability change for this mode can be calculated from the Clausius-Mossotti relation

$$\alpha=(3\epsilon_0/N)[(n^2-1)/(n^2+2)] . \quad (31)$$

The refractive index change arising from a Nb^{5+} ion hopping between the two nonequivalent potential wells is inferred from the linear birefringence for $KNbO_3$ crystals.[33] At 300 K Δn is approximately 0.18 and it decreases to about 0.15 at 500 K. Substituting for the measured Raman peak linewidth and the calculated value of $\Delta\alpha$ the contribution to $\chi^{(3)}$ is 9×10^{-13} esu. Stimulated hopping between two of the equivalent potential wells will make a similar contribution to $\chi^{(3)}$.

The intensity of the diffracted signal was measured as a function of temperature for undoped $KNbO_3$ and the results are shown in Fig. 13. The signal was measured at two delay times of the probe pulse, 0 and 150 psec. The results at zero delay show the signal strength to decrease as temperature is increased while the signal at 150 psec increases very slightly. A larger temperature range could not be studied because of the phase transitions of the crystal at 250 K. The intensity of the Raman-scattering peak was observed to increase with temperature.[28] This peak is associated with relaxations from the higher-energy potential well to the lower well which will become more probable as the upper well is thermally activated. In terms of the zero-delay signal observed in our laser-induced grating experiment where the light pattern is driving the modes in the bright regions, the detected signal intensity depends on the contrast in the refractive index between the bright and dark regions of the sample. As the temperature is increased this contrast decreases as the Nb^{5+}-phonon modes become more occupied in the dark regions. Also the linear birefringence between the two phases decreases as the temperature increases.[33] The decrease in Δn is about 17% over the temperature range between 300 and 500 K while the signal decrease in the same range is close to 28%.

Thus from the above discussion it appears that the bound electron and Nb-hopping mode both contribute to the observed FWM signals at zero time delay in $KNbO_3$. Further experiments using different samples and faster excitation pulses will be done to separate these contributions.

ACKNOWLEDGMENTS

This work was sponsored by the Army Research Office. The authors benefitted greatly from discussions with G. C. Valley and with L. L. Chase concerning the Nb-hopping modes and his Raman-scattering results.

*Permanent address: Department of Physics, Central State University, Edmond, Oklahoma 73060.

[1]P. Gunter, Phys. Rep. **93**, 199 (1982).
[2]P. Gunter and J. P. Huignard, in *Photorefractive Materials and their Applications I,* edited by P. Gunter and J. P. Huignard (Springer-Verlag, Berlin, 1988), p. 65.
[3]P. Gunter, Opt. Commun. **11**, 285 (1974).
[4]G. J. Mizell, W. R. Fay, and Y. Shimoji, SPIE **968**, 88 (1988).
[5]E. Voit, M. Z. Zha, P. Amrhein, and P. Gunter, Appl. Phys. Lett. **51**, 2079 (1987).
[6]J. P. Huignard and A. Marrakchi, Opt. Commun. **38**, 249 (1981).
[7]M. B. Klein and G. C. Valley, J. Appl. Phys. **57**, 4901 (1985).
[8]E. Wiesendanger, Ferroelectrics **6**, 263 (1974).
[9]G. D. Boyd, R. C. Miller, K. Nassau, W. L. Bond, and A. Savage, Appl. Phys. Lett. **5**, 234 (1964).
[10]N. Kukhtarev, V. Markov, and S. Odulov, Opt. Commun. **23**, 338 (1977).
[11]N. V. Kukhtarev, Pis'ma Zh. Tekh. Fiz. **2**, 1114 (1976) [Sov. Tech. Phys. Lett. **2**, 438 (1976)].
[12]G. C. Valley, J. Appl. Phys. **59**, 3363 (1986).
[13]F. P. Strohkendl, J. M. C. Jonathan, and R. W. Hellwarth, Opt. Lett. **11**, 312 (1986).
[14]H. Kogelnik, Bell Syst. Tech. J. **48**, 2909 (1969).

[15]C. Medrano, E. Voit, P. Amrhein, and P. Gunter, J. Appl. Phys. **64**, 4668 (1988).
[16]A. L. Smirl, G. C. Valley, R. A. Mullen, K. Bohnert, C. D. Mire, and T. F. Boggess, Opt. Lett. **12**, 501 (1987).
[17]A. L. Smirl, K. Bohnert, G. C. Valley, R. A. Mullen, and T. F. Boggess, J. Opt. Soc. Am. B **6**, 606 (1989).
[18]R. B. Bylsma, D. H. Olson, and A. M. Glass, Opt. Lett. **13**, 853 (1988).
[19]R. A. Mullen, Ph.D. thesis, University of Southern California, 1984 (unpublished).
[20]K. Tyminski and R. C. Powell, J. Opt. Soc. Am. B **2**, 440 (1985).
[21]J. M. C. Jonathan, G. Roosen, and Ph. Roussignol, Opt. Lett. **13**, 224 (1988).
[22]G. C. Valley, A. L. Smirl, M. B. Klein, K. Bohnert, and T. F. Boggess, Opt. Lett. **11**, 647 (1986).
[23]M. S. Petrovic, A. Suchocki, R. C. Powell, G. Cantwell, and J. Aldridge, J. Appl. Phys. **66**, 1359 (1989).
[24]A. Yariv and R. A. Fisher, in *Optical Phase Conjugation,* edited by R. A. Fisher (Academic, London, 1983), p. 14.
[25]J. D. Jackson, in *Classical Electrodynamics,* 2nd ed. (Wiley, New York, 1975), p. 272.
[26]R. K. Jain, Opt. Eng. **21**, 199 (1982).
[27]R. Adair, L. L. Chase, and S. A. Payne, Phys. Rev. B **39**, 3337 (1989).
[28]J. P. Sokoloff, L. L. Chase, and D. Rytz, Phys. Rev. B **38**, 597 (1988).
[29]M. D. Fontana, A. Ridah, G. E. Kugel, and C. Carabatos-Nedelec, J. Phys. C **21**, 5853 (1988).
[30]M. D. Fontana, G. E. Kugel, and C. Carabatos-Nedelec, Phys. Rev. B **40**, 786 (1989).
[31]J. P. Sokoloff, L. L. Chase, and D. Rytz, Phys. Rev. B **40**, 788 (1989).
[32]L. L. Chase (private communication).
[33]W. Kleemann, F. J. Schafer, and M. D. Fontana, Phys. Rev. B **30**, 1148 (1984).